THE ASTROPHYSICAL JOURNAL, 446:457–471, 1995 June 20

THE OPTICAL REDSHIFT SURVEY: SAMPLE SELECTION AND THE GALAXY DISTRIBUTION[1]

BASÍLIO X. SANTIAGO,[2] MICHAEL A. STRAUSS,[3] OFER LAHAV,[2] MARC DAVIS,[4]
ALAN DRESSLER,[5] AND JOHN P. HUCHRA[6]

Received 1994 June 20; accepted 1995 January 6

ABSTRACT

This is the first in a series of papers describing the Optical Redshift Survey (ORS), a redshift survey of optically selected galaxies covering 98% of the sky above $|b| = 20°$ (8.09 sr). The survey is drawn from the Uppsala Galaxy Catalogue (UGC), the European Southern Observatory Galaxy Catalogue (ESO), and the Extension to the Southern Galaxy Catalogue (ESGC), and it contains two subcatalogs, one complete to a B magnitude of 14.5, the other complete to a B major axis diameter of 1'.9. The entire sample consists of 8457 objects, of which redshifts are now available for 8286; 171 objects remain without measured redshifts. Roughly 1300 of the redshifts were measured for the completion of the sample; the remainder were taken from the literature. Most of these new redshifts are concentrated at low Galactic latitudes, $20° \leq |b| \leq 30°$, and within the strip not covered by either the UGC or ESO catalogues: $-17°.5 \leq \delta \leq -2°.5$. The ORS provides the most detailed and homogeneous sampling of the large-scale galaxy distribution to date in these areas. The density field of bright optical galaxies is well defined to 8000 km s^{-1} and is dominated by the Virgo, Hydra-Centaurus, Pisces-Perseus, Coma-A1367, and Telescopium-Pavo-Indus superclusters. The dense sampling provided by ORS allows a detailed analysis of the galaxy density field and will be used to test its dependence on morphology and other galaxy parameters.

Subject headings: cosmology: observations — galaxies: clusters: general — galaxies: distances and redshifts — surveys

1. INTRODUCTION

Despite the immense increase in the number of galaxy redshifts measured in the past decade, there is much to learn from well-defined complete redshift surveys of nearby galaxies. The global mean density of galaxies may still have significant uncertainties owing to the presence of large-scale structure comparable in size to the samples themselves (de Lapparent, Geller, & Huchra 1988; da Costa et al. 1994); the measurement of various high-order galaxy clustering statistics are limited by the finite volumes and sparse sampling of existing surveys (Bouchet et al. 1993; Fisher et al. 1994b), and little is known quantitatively about the relative distribution of galaxies of different morphological types on very large scales.

The first complete redshift survey to cover both Galactic hemispheres was that of Yahil, Sandage, & Tammann (1980), which mapped the Local Supercluster using the galaxies of the Revised Shapley-Ames Catalog (Sandage & Tammann 1981, hereafter RSA). Analyses of the optical extragalactic sky were carried out using a compilation of the Uppsala Galaxy Catalogue (UGC), European Southern Observatory Galaxy Catalogue (ESO), and Morphological Catalogue of Galaxies (MCG) catalogs in two dimensions (Lahav 1987; Lahav, Rowan-Robinson, & Lynden-Bell 1988); Lynden-Bell, Lahav, & Burstein (1989, hereafter LLB) and Hudson (1993a, b) used partial redshift information with statistical corrections for incompleteness to map the three-dimensional density field. When the database of the *Infrared Astronomical Satellite* (*IRAS*) was produced, several groups used it as a target list to carry out flux-limited, almost full-sky redshift surveys of galaxies, which probed considerably beyond the Local Supercluster (Strauss et al. 1990, 1992b; Fisher et al. 1995; Rowan-Robinson et al. 1990; Lawrence et al. 1994; Saunders et al. 1995a). These surveys have been used to trace the large-scale distribution of galaxies within 20,000 km s^{-1} of the Local Group (Saunders et al. 1991; Strauss et al. 1992a) and thus predict the peculiar velocity field via gravitational instability theory (Yahil et al. 1991; Kaiser et al. 1991; Strauss et al. 1992c; Dekel et al. 1993; cf. Strauss 1993; Dekel 1994; Strauss & Willick 1995 for reviews of scientific results from these surveys).

The dynamical inferences from the *IRAS* galaxy redshift surveys have been called into question, however, because of our lack of knowledge of the relative distribution of galaxies and mass. Moreover, *IRAS* galaxies are predominantly star-forming, dusty, late-type galaxies and are underrepresented in cores of rich clusters relative to optically selected galaxies (Strauss et al. 1992a and references therein). Indeed, on scales of 800 km s^{-1}, the rms fluctuation in the *IRAS* counts are smaller than those of optical galaxies by a factor of 1.3–1.5 (e.g., Lahav, Nemiroff & Piran 1990; Scharf et al. 1992; Strauss et al. 1992a; Saunders, Rowan-Robinson & Lawrence 1992; Fisher et al. 1994a).

[1] Based in part on data obtained at Lick Observatory, operated by the University of California; the Multiple Mirror Telescope, a joint facility of the Smithsonian Astrophysical Observatory and the University of Arizona; Cerro Tololo Inter-American Observatory, operated by the Association of Universities for Research in Astronomy, Inc., under contract with the National Science Foundation; Palomar Observatory, operated by the California Institute of Technology, the Observatories of the Carnegie Institution, and Cornell University; and Las Campanas Observatory, operated by the Observatories of the Carnegie Institution.

[2] Institute of Astronomy, Cambridge University, Madingley Road, Cambridge, England, UK CB3 0HA.

[3] Institute for Advanced Study, School of Natural Sciences, Princeton, NJ 08540.

[4] Physics and Astronomy Departments, University of California, Berkeley, CA 94720.

[4] Observatories of the Carnegie Institution of Washington, 813 Santa Barbara Street, Pasadena CA 91101.

[6] Center for Astrophysics, 60 Garden Street, Cambridge, MA 02138.

However, it is still unclear if these differences extend to larger scales, and to what extent such differences affect various measures of large-scale structure. For example, the dipole moment of the galaxy density field can be compared with motion of the Local Group with respect to the cosmic microwave background in order to measure $\beta \equiv \Omega^{0.6}/b$, where Ω is the cosmological density parameter and b is the bias factor. Lahav et al. (1988), Hudson (1993a, b), Freudling & da Costa (1994), and Hudson et al. (1995) have argued that β for optical galaxies is smaller by a factor of 2 than that derived from *IRAS* galaxies. Strauss et al. (1992a) argued that *IRAS* and optically selected galaxies traced the same large-scale structures, although Santiago & Strauss (1992) found significant difference between optically selected galaxies of different Hubble types (see Lahav & Saslaw 1992). Motivated by these ambiguities, we undertook a new redshift survey of optically selected galaxies covering most of the celestial sphere. We call it the Optical Redshift Survey, or ORS. Our principal motivation is to quantify any possible differences between the large-scale structure as defined by *IRAS* and optically selected galaxies. In addition, we wish to look for morphological segregation on large scales between galaxies of different morphological types. Our hope is that this will give new insights into the process of galaxy formation and possible biasing of the galaxy distribution relative to that of mass on very large scales, while testing many of the results based on the *IRAS* density field.

The *IRAS* redshift surveys have the advantage of an approximately uniform selection over the entire sky (see the discussion in *IRAS* 1988; Strauss et al. 1990), while any optically selected survey necessarily is strongly affected by the zone of avoidance, and the presence of extinction at low Galactic latitudes. In Santiago et al. (1995; hereafter Paper II), we will outline methods to correct for these problems. However, the ORS is much more densely sampled than is the *IRAS* survey, meaning that structures can be delineated and quantified with less noise on any given smoothing scale. Moreover, the ORS includes the early-type galaxies that are not represented in the *IRAS* survey.

This is the first in a series of papers presenting results from the ORS. We define the sample in § 2, and in § 3 we show the redshift data using a variety of projections. Quantitative results from this survey will be presented in a series of papers in preparation, as outlined in § 4. The data themselves will be published in the near future.

2. SAMPLE DEFINITION

2.1. *The Catalogs Used*

There exists no single galaxy catalog selected from optical plate material deeper than the RSA, which covers both halves of the celestial sphere. For this reason, we have selected our redshift sample from three different galaxy catalogs, as follows:

In the southern sky defined by $\delta \leq -17.^\circ5$[7] we used the ESO-Uppsala Survey of the ESO(B) Atlas (Lauberts 1982; ESO), as well as its photometric counterpart, the Surface Photometry Catalogue of the ESO-Uppsala Galaxies (Lauberts & Valentijn 1989; ESO-LV). The ESO catalog is nominally complete in apparent visual diameters, measured from the ESO(B) Survey plates down to $\theta \geq 1'$ (see Hudson & Lynden-Bell 1991, hereafter HLB, who show that the completeness limit is closer to 1.'35). The ESO-LV consists of the results of photodensitometer scans of these galaxies from the ESO(B) and ESO(R) plates (although it is not complete; see below) and tabulates magnitudes, diameters, and surface brightnesses. ESO-LV also contains data on a number of companion objects to the original ESO galaxies, as well as on many individual components of multiple systems of galaxies. The listed positions of the galaxies are accurate to $\sim 6''$ (Lauberts 1982).

In the northern sky ($\delta \geq -2.^\circ5$), galaxies were selected from the Uppsala General Catalogue of Galaxies (Nilson 1973; UGC). This data set is also nominally complete for $\theta \geq 1'$, as measured by eye from the Palomar Sky Survey (POSS) 103a-O plates, although HLB show that the actual completeness limit is closer to $\sim 1.'65$. The UGC also includes all galaxies with apparent B-band magnitude $m_B \leq 14.5$ as listed in the Catalog of Galaxies and Clusters of Galaxies (Zwicky et al. 1961–1968, hereafter CGCG). The CGCG is nominally complete to $m_B \leq 15.5$ and covers the same area on the sky as the UGC, except for regions close to the Galactic plane. The UGC galaxy positions are of varying quality, and so we updated them with positions from the NASA Extragalactic Database (NED). In addition, we corrected typographical errors in the ESO and UGC catalogs following Paturel et al. (1991) and private communications with H. Corwin.

Galaxies in the strip between the ESO and UGC regions, ($-17.^\circ5 \leq \delta \leq -2.^\circ5$) were sampled using the recently completed Extension to the Southern Galaxies Catalogue (Corwin & Skiff 1994, hereafter ESGC). We hereafter refer to this region of sky as the ESGC strip. The ESGC actually covers the region $-21^\circ \leq \delta \leq 3^\circ$ and is complete to major axis diameters of 1.'9 (see below) as measured by eye on the POSS 103a-O plates. The positions in this catalogue are accurate to a few arcseconds in most cases; several positions were updated by B. X. S. An alternate sample in this region of the sky is the MCG (Vorontsov-Velyaminov, Archipova, & Krasnogorskaja 1962–1974), but the photometry and astrometry of this sample are known to be of poor quality. A previous redshift survey of this region has been carried out by Pellegrini et al. (1990) and Huchra et al. (1993).

The completeness of the ESGC is demonstrated in Figure 1, which shows the cumulative distribution of major axis diameters of the sample. In the absence of clustering, the distribution is expected to be proportional to θ^{-3} to the completeness limit. The dashed line shows this expected distribution, which indeed is an excellent fit for diameters larger than 1.'9, indicating that the sample is complete to this limit. The sample does include a small number of galaxies with smaller diameters, which is why the cumulative curve does not become flat beyond this limit. Our redshift sample is limited exclusively to objects larger than 1.'9.

The dashed line fits the data poorly for diameters larger than 5'; this is presumably due to large-scale structure and shot noise. See HLB for similar plots for the ESO and UGC samples.

2.2. *Sample Selection*

We wish to have a sample covering as much of the celestial sphere as possible. Examination of the Galactic extinction maps of Burstein & Heiles (1982, hereafter BH) shows that there are few regions at Galactic latitudes higher than $|b| = 20^\circ$ with excessive extinction, and thus we decided to limit our survey at this latitude. In addition, we excluded the regions of the sky at higher latitude in which the B-band extinction according to BH was greater than $A_B = 0.7$ mag (this excludes only 0.18 sr). Approximate borders expressed in

[7] All positions in this paper are B1950.

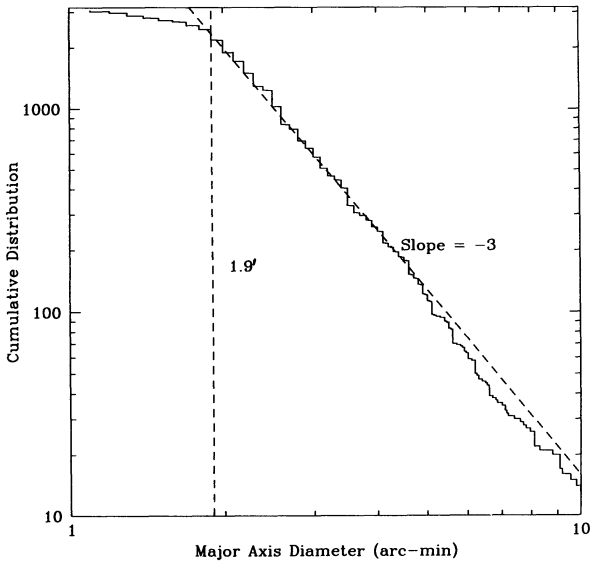

FIG. 1.—Cumulative apparent diameter distribution of galaxies in the ESGC. The dashed line represents the expected distribution under the assumption that galaxies are uniformly distributed in space.

Galactic coordinates for these high-extinction regions are listed in Table 1. It is worth pointing out that the BH maps are based on H I maps and galaxy counts that go many magnitudes deeper than does our sample, and a scatter plot of the extinction values with the derived surface density shows no correlation at all, as we would expect. Galaxies in the remainder of the celestial sphere were then selected from the catalogs listed above, according to the union of the following criteria:

1. $\theta \geq 1'.9$, where θ is an apparent major axis diameter. For the ESO part of the sky, θ corresponds to the original ESO B-band diameter rather than to any of the isophotal ESO-LV measurements, as this is the quantity by which ESO was limited. We did not correct diameters to face-on (see da Costa et al. 1988); major-axis diameters were used throughout.

2. $m_B \leq 14.5$, where m_B is an apparent magnitude in the B band. For ESO, we used the ESO-LV total magnitudes, B_T.

TABLE 1

APPROXIMATE BOUNDARIES OF HIGH EXTINCTION EXCLUDED ZONES

l	b
$0° \leq l \leq 14°$	$+20° \leq b \leq +30°$
$165 \leq l \leq 187$	$-40 \leq b \leq -20$
$203 \leq l \leq 215$	$-25 \leq b \leq -20$
$279 \leq l \leq 287$	$-25 \leq b \leq -20$
$288 \leq l \leq 297$	$-30 \leq b \leq -25$
$340 \leq l \leq 360$	$+20 \leq b \leq +30$

Galaxies with ESO B-band diameters less than 1′ were excluded, even if they were brighter than the nominal flux limit, as the ESO sample is incomplete below 1′. For UGC, CGCG magnitudes were used, as listed in the UGC itself; for those objects in the UGC without CGCG magnitudes, magnitudes were estimated by Nilson. There are no magnitudes (other than the very poor ones from the MCG) available in the ESGC strip. The CGCG magnitudes are known to be systematically 0.3 mag too faint in Volume 1 of the CGCG ($7^h < \alpha < 18^h$, $-2°.5 < \delta < 15°$) (Kron & Shane 1976; Paturel 1977; Fasano 1985); we correct for this effect in Paper II.

For all parts of the sky, we select our sample according to *observed* magnitudes or diameters as listed in the machine-readable versions of the catalogs. In particular, in defining the sample we do not correct the magnitudes and diameters for Galactic or internal extinction, nor do we apply corrections to bring the various photometric systems into agreement (see LLB). It is known, for instance, that the ESO diameter scale differs systematically from that of the UGC (Lahav et al. 1988; HLB; see below). Corrections for these effects will be applied in the analysis stage by incorporating them in the sample selection function (Paper II). However, we can use the overlap between the samples to compare the relative diameter scales, even if we will not use this information here. Figure 2 compares the ESGC diameter scale with that of ESO and UGC for those galaxies in common. Note the logarithmic axes. The paucity of points below $D_{ESGC} = 114'' = 1'.9$ is just a reflection of the completeness limit of this catalog. In each panel, the solid line is $y = x$, while the dashed line is the best fit to $y = cx$. Thus, we

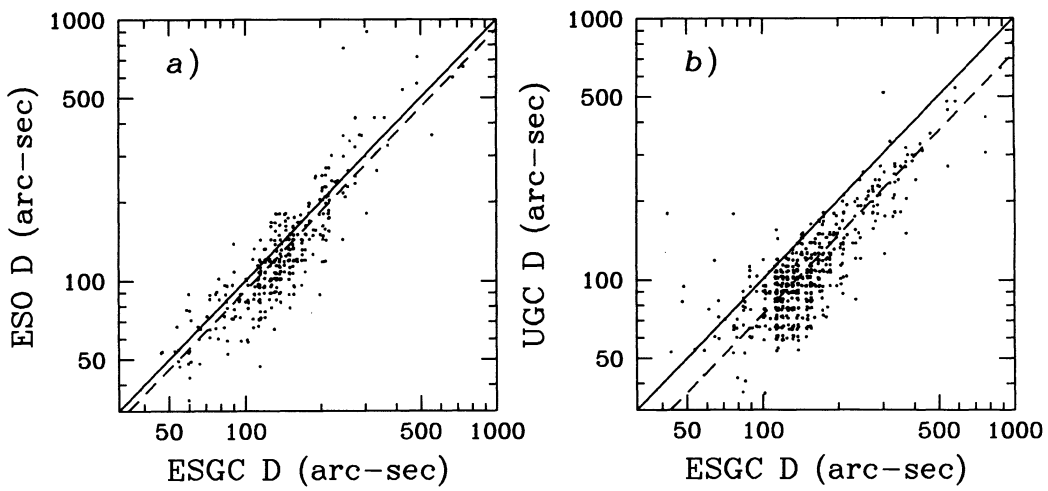

FIG. 2.—(*a*) Correlation between the original ESO diameters and the ESGC diameters for the 347 objects in common between the two data sets. (*b*) Same as (*a*) for the 595 galaxies in common between UGC and ESGC.

find that

$$D_{\rm ESO} = (0.918 \pm 0.014) D_{\rm ESGC}\,, \quad (1)$$

$$D_{\rm UGC} = (0.735 \pm 0.010) D_{\rm ESGC}\,, \quad (2)$$

implying that

$$D_{\rm ESO} = (1.249 \pm 0.026) D_{\rm UGC}\,. \quad (3)$$

LLB determined this latter ratio by fitting diameter functions to the ESO and UGC diameters; they obtained $D_{\rm ESO}/D_{\rm UGC} = 1.17 \pm 0.07$, which is consistent with equation (3) within the error bars. Note that there is some evidence for a logarithmic slope steeper than unity in the UGC-ESGC comparison; there may be nonlinearities in the UGC diameter scale. Furthermore, the fits may be slightly affected by Malmquist bias, owing to the limit in the ESGC diameters. However, Monte Carlo experiments show this to be only a $\sim 5\%$ effect in the ratio. Other comparisons between different diameter systems, including UGC and ESO, have been carried out by Fouqué & Paturel (1985), Paturel et al. (1987), de Vaucouleurs et al. (1991), and Saunders et al. (1995b).

In Figure 3 we compare the original ESO diameters measured by eye to those from ESO-LV measured at the $B = 26$ mag per square arcsecond isophote. There is good agreement between the two diameter scales, although at very small diameters (well below the ORS diameter limit), the ESO-LV diameters are systematically larger.

Another important issue in defining the ORS is the presence of binaries or multiple systems of galaxies with a single entry in the catalogs. These were excluded from the sample, unless magnitudes or diameters were available for individual components which satisfied the ORS selection criteria. Information on individual galaxies in multiple systems is available in the ESO-LV database; wherever the individual galaxies satisfied our selection criteria, we included them in our sample. We searched the notes section of the UGC for the 125 entries classified as multiple and whose system diameters or magnitudes were large enough to make it onto ORS; only seven of them had components whose individual magnitudes and diameters caused them to enter our sample. For the ESGC, separation of individual galaxies in multiples has not yet been carried out, and we excluded the 59 entries classified as unseparated multiples and carefully checked the sample for duplicate entries. We thank Harold Corwin for his help in sorting out all doubtful cases.

Thus, we have two complete, although somewhat nonuniform, samples: a diameter-limited sample covering the whole sky (other than those regions for which $A_B > 0.7$) for $|b| > 20°$, which we refer to as ORS-d, and a magnitude-limited sample covering essentially the same area minus the ESGC strip, which we refer to as ORS-m. We refer to the corresponding subsamples covering only the ESO region of the sky as ESO-d and ESO-m, and similarly for the UGC. As no magnitudes are available for the ESGC region, we refer to its diameter-limited subsample simply as ESGC. There is of course very substantial overlap between the ORS-m and ORS-d samples.

In Table 2 we provide information about the various ORS subsamples: sample designations are given in column (1), selection criteria are in column (2), and solid angles are in column (3). The total numbers of objects are given in column (4), while

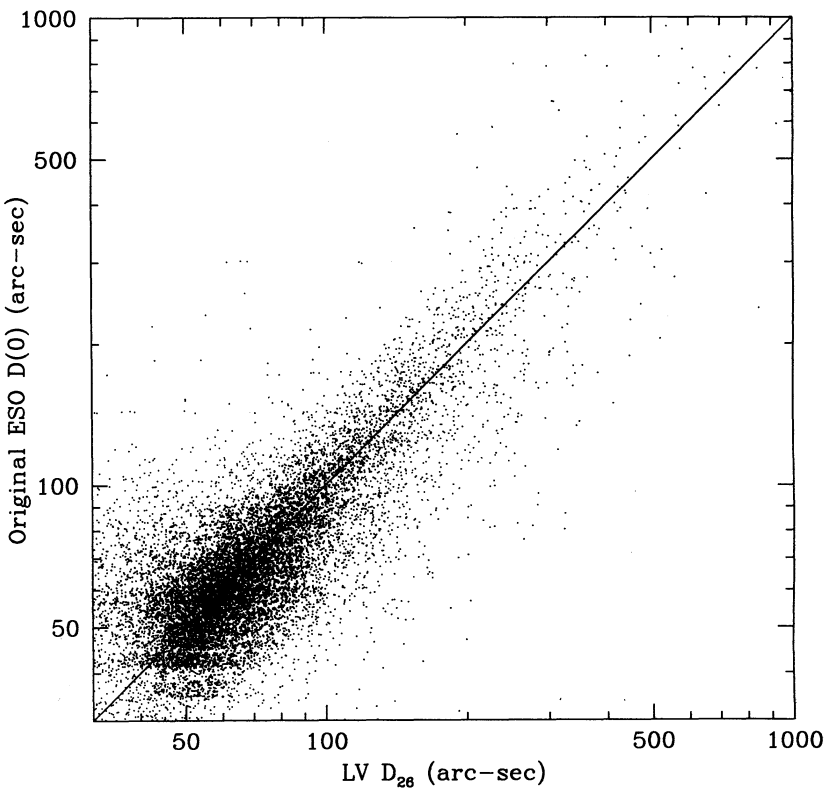

FIG. 3.—The relation between the original ESO diameters and those corresponding to the 26th magnitude isophotal level in *B* from ESO-LV. All ESO-LV galaxies for which the latter is available are plotted, for a total of 14864 objects.

TABLE 2

OPTICAL REDSHIFT SURVEY SUBSAMPLES

Catalog (1)	Cutoff (2)	Solid Angle (sr) (3)	Number of Objects (4)	Number with z (5)	Completeness (6)
ESO-d	$\theta \geq 1.^{\circ}9$	2.70	1845	1821	0.987
ESO-m	$B_T \leq 14.5$	2.37	2437	2425	0.995
ESGC	$\theta \geq 1.^{\circ}9$	1.14	1454	1353	0.931
UGC-d	$\theta \geq 1.^{\circ}9$	4.25	2035	2002	0.984
UGC-m	$m_B \leq 14.5$	4.25	3279	3272	0.998
ORS-m	$m_B \leq 14.5$	6.62	5716	5697	0.997
ORS-d	$\theta \geq 1.^{\circ}9$	8.09	5334	5176	0.970
ORS-m ∪ ORS-d	...	8.09	8457	8286	0.980

the number and fraction with measured redshifts are in columns (5) and (6), respectively. The final entry in Table 2 gives numbers for the union of ORS-m and ORS-d.

Unfortunately, ESO-LV magnitudes do not exist for the entire sky south of $\delta < -17.^{\circ}5$; there remain 64 plates that at least partially cover the region $|b| > 20°$ and were not scanned. Thus, the ESO-m sample covers a small solid angle than does the ESO-d (see Table 2). In order to define the excluded zones unambiguously, we exclude any ESO-m galaxy if its right ascension or declination falls within $2.^{\circ}5$ of the center of one of these 64 plates, even if it enters the catalog from an overlapping plate. Notice also that there is a diameter selection inherent in ESO-m, as it does not include galaxies brighter than $B_T = 14.5$ but smaller than the original ESO diameter limit. The UGC-m sample does not suffer from this problem: it is the union of a diameter-limited sample and the subset of the CGCG catalog with $m_B \leq 14.5$.

As the ORS sample as defined above consists of bright and/or large galaxies, the majority had redshifts available in the literature, in particular from the CfA (Huchra et al. 1983), CfA2 (Huchra et al. 1990), Southern Sky Redshift Survey (SSRS) (da Costa et al. 1991), SPS (Dressler 1991), MCG Equatorial (Huchra et al. 1993) and *IRAS* (Strauss et al. 1992b; Fisher et al. 1995; Lawrence et al. 1994) redshift surveys. In practice, we matched the catalog against a private version of the redshift compilation of J. P. H. (ZCAT). This left approximately 1300 redshifts unmeasured, largely concentrated in the regions of sky not previously covered by redshift surveys: the ESGC strip and the two strips defined by $20° < |b| < 30°$. These redshifts were measured over 4 years at Palomar, Lick, Mount Hopkins, Las Campanas, and Cerro Tololo Inter-American Observatories. The typical error in these redshifts was 50 km s^{-1}. The details of the observing runs and the reduction procedures will be given in our data paper.

The completeness of the redshift survey is excellent: above 98% for all subsamples except for the ESGC strip (93.1%). The (diameter-limited) ESGC sample includes many very low surface brightness galaxies for which it is very difficult to measure a redshift. The ESO-d sample was defined in terms of visually estimated diameters, but because of the good correlation with isophotal diameters from ESO-LV (Fig. 3), a sample defined by ESO $D_{26} \geq 1.^{\circ}9$ is still ~95% complete in redshift.

Figure 4 shows the redshift distribution of the different subsamples normalized by their respective solid angles. Each subsample shows the effects of large-scale structure. The UGC-m is noticeably deeper than is the ESO-m sample. The peak at 1000 km s^{-1} in the UGC-m is due to the Ursa Major and Virgo clusters. Six thousand km s^{-1} is roughly the redshift at which an L_* galaxy will be at the magnitude limit of the sample, causing the peak there; the very sharp fall-off at larger distances is a reflection of the exponential tail of the optical galaxy luminosity function (Schechter 1976; Loveday et al. 1992, and references therein). The ESGC is of comparable depth to the UGC-m, but is more densely sampled by a factor of 2 (which may partly be due to large-scale structure; the peak at 2000–3000 km s^{-1} is due to the Great Attractor region). All three samples cut off abruptly at 10,000 km s^{-1}. The UGC-d and ESO-d subsamples are also shown; their cutoff at high redshift is not as strong as that for the magnitude-limited subsamples, and the redshift distribution is much flatter. In addition, the diameter-limited subsamples are quite a bit more sparsely sampled than are the magnitude-limited subsamples. For comparison, the *IRAS* 1.2 Jy sample (Fisher et al. 1995) has a redshift distribution that peaks at a comparable redshift to that of UGC-m, but it has a high-redshift tail that extends appreciably farther than do the optical surveys. This is a reflection of the power-law tail of the *IRAS* luminosity function at high luminosities, in contrast with the exponential cutoff of the optical luminosity and diameter functions. As discussed in the Introduction, the *IRAS* sample is substantially sparser than are the optically selected samples.

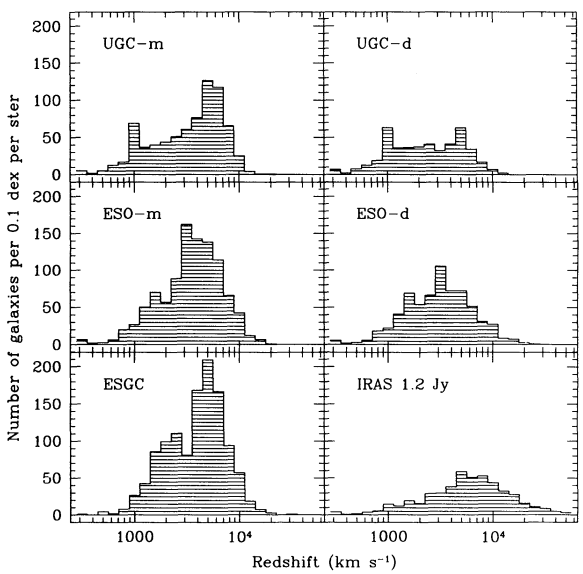

FIG. 4.—Redshift distributions for the different ORS subsamples. The distribution for the *IRAS* 1.2 Jy survey is also shown for comparison. The number of galaxies in each subsample has been normalized by the respective solid angles, and is shown in logarithmic bins of width 0.1 dex.

3. THE DISTRIBUTION OF GALAXIES IN THE SURVEY

3.1. *Distribution on the Sky*

Before showing the sky distribution of the data themselves, Figure 5*a* shows the geometry of the survey in an Aitoff projection of the sky in Galactic coordinates. The hatched region at low Galactic latitudes is the zone of avoidance, $|b| < 20°$, while the higher latitude black areas correspond to those regions with $A_B > 0.7$. They occupy only 2% of the sky outside of the zone of avoidance, or 0.18 sr. The two largest such areas are in Orion ($l = 150°$–$190°$, $b = -30°$) and near the Galactic center ($l = 330$–$30°$, $b = 20$–$30°$). The grey areas at high Galactic latitude are the plates not surveyed by ESO-LV; these represent excluded zones for the ESO-m sample, but not the ESO-d. They cover an additional 0.33 sr, or 4% of the high-latitude sky. The two S-shaped lines are drawn at $\delta = -2°.5$ and $\delta = -17°.5$, respectively, and mark the boundaries between the ESO, ESGC, and UGC samples. Figure 5*b* shows the distribution of those galaxies for which we were unable to measure redshifts. The highest concentration of these is in the ESGC strip, again indicated with two S-shaped lines. We attempted to measure redshifts for most of these objects, but the majority of them were of very low surface brightness. In the ESO and UGC regions, most of the galaxies without redshifts are in the diameter-limited sample and are also of very low surface brightness. There were also some galaxies with bright stars superposed for which we were unable to obtain a spectrum.

In order to present the data themselves, we use the union of the UGC-m, ESO-m, and ESGC data. The description here will be qualitative; more systematic and quantitative analysis of the data will be presented in the upcoming papers of this series.

Figure 6*a* shows the distribution of the entire sample on the celestial sphere using an equal-area polar hemispheric projection in Galactic coordinates (Lahav 1987; Scharf & Lahav 1993). The circle on the left (right) side corresponds to the north (south) Galactic hemisphere. The poles are at the center of these circles with Galactic latitude decreasing radially outward; the dashed circles are drawn at Galactic latitudes 20°, 40°, 60°, and 80° in the north, and −20°, −40°, −60° and −80° in the south. Galactic longitude runs azimuthally as indi-

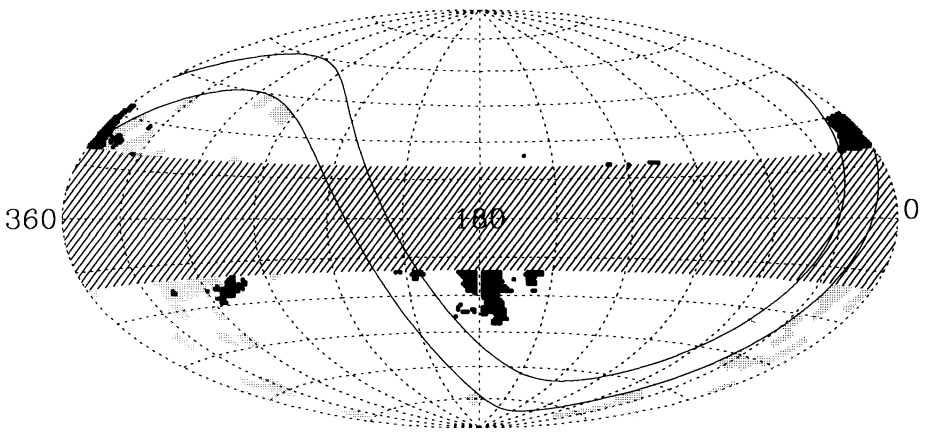

FIG. 5*a*

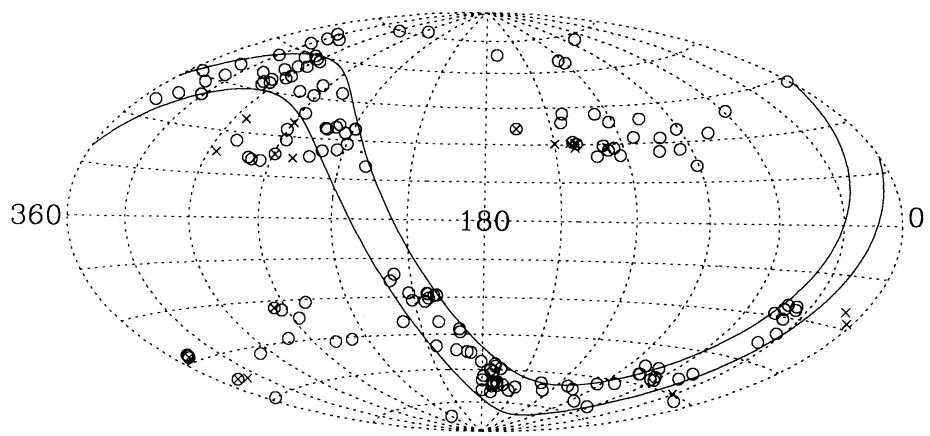

FIG. 5*b*

FIG. 5.—(*a*) Regions not covered by ORS are shown in an Aitoff projection on the sky using Galactic coordinates. The horizontal strip corresponds to the zone of avoidance ($|b| \leq 20°$). The heavy lines mark the boundaries of the ESGC strip. The dark areas correspond to high-extinction regions ($A_B > 0.7$ mag) and the grey ones to those plates in the southern sky not surveyed by the ESO-LV and therefore not covered by ESO-m. (*b*) ORS galaxies for which no redshift is yet available are shown in an Aitoff projection on the sky. Galaxies belonging to ORS-m are indicated by crosses, and those in ORS-d by open circles. Most of the missing redshifts are in ORS-d and correspond to faint or low surface brightness galaxies. The ORS region with the largest degree of incompleteness is the ESGC strip, which is contained within the two heavy lines. There are 171 galaxies in all without redshifts.

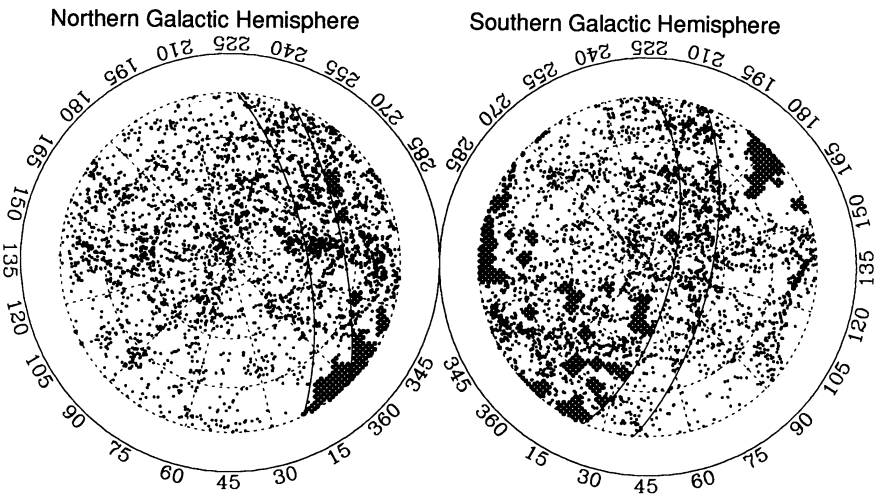

FIG. 6a

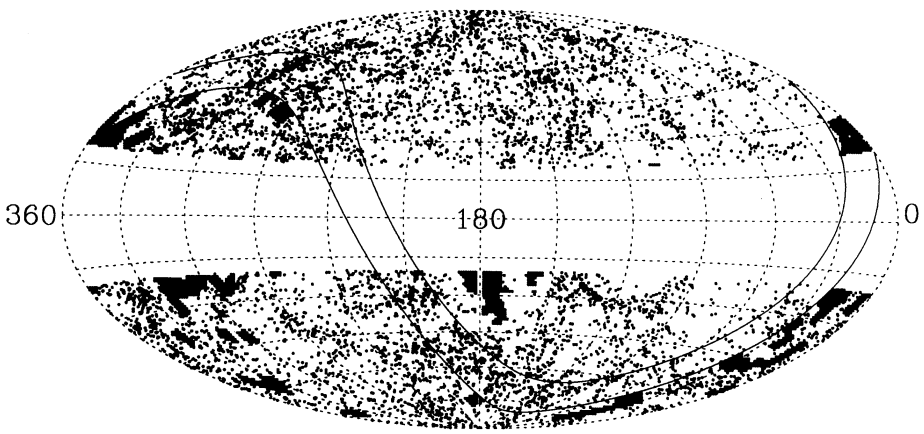

FIG. 6b

FIG. 6.—(*a*) The ORS sample shown in polar projections of the two Galactic hemispheres. The circle on the left (right) corresponds to the north (south) Galactic hemisphere, as indicated. Galactic latitude decreases radially from the center of each panel, whereas Galactic longitude runs in azimuth. The dashed circles are at constant Galactic latitude and are spaced every 20° starting at $b = 20°$ and $b = -20°$. The outer rings devoid of galaxies in both hemispheres correspond to the zone of avoidance. The two heavy lines in each circle demark the ESGC strip. The excluded regions are indicated with hatching (compare Fig. 5*a*). (*b*) As in (*a*), now in Aitoff projection.

cated. The circles are rotated so as to make the supergalactic plane (SGP) stretch along the horizontal direction. The shaded regions correspond to the excluded zones (compare with Fig. 5*a*). The ESGC strip is marked with two solid lines in both hemispheres. The outer ring devoid of galaxies is the zone of avoidance ($|b| < 20°$).

Interpretation of structures in this map is difficult: each subsample making up the survey has a different selection function (Fig. 4), large-scale Galactic extinction creates artificial low-density regions, and the projection of all the data tends to wash out features. However, a few structures catch the eye immediately: the densest part of the Local Supercluster and the Hydra-Centaurus supercluster is prominent in the Northern Hemisphere at $l = 300°$–$315°$ from $b = 20°$ almost to the North Pole. It appears to be contiguous with the TPI supercluster in the Southern Hemisphere. The Pisces-Perseus chain is also visible at $l = 105°$–$135°$ and $b = -30°$.

Figure 6*b* shows the same data, now in an Aitoff projection. This complementary projection of the data makes clearer the relation of structures to one another near the Galactic plane, but of course distorts features near the poles. Again, the plane of the Local Supercluster, the TPI supercluster, and Pisces-Perseus supercluster are all apparent. The lower density of galaxies at small Galactic longitudes is largely due to Galactic extinction.

In order to distinguish structures more clearly, we make use of our redshift data, plotting the galaxies in constant redshift slices. For each slice, we show two figures, one in hemispherical projection, as in Figure 6*a*, and one in Aitoff projection, as in Figure 6*b*. In each case, we also show the galaxy density field on a constant redshift shell, smoothed with a Gaussian whose width increases proportional to the mean interparticle separation. Contrary to the galaxy maps, these contour densities are corrected for extinction, the excluded zones, the selection function of each catalog, and other related effects; details are in Paper II.

The upper panels of Figures 7*a* and 7*b* show the galaxy distribution of galaxies with redshifts (corrected for the motion of the Sun relative to the barycenter of the Local Group following Yahil, Tammann, & Sandage 1977) between 0 and 3000

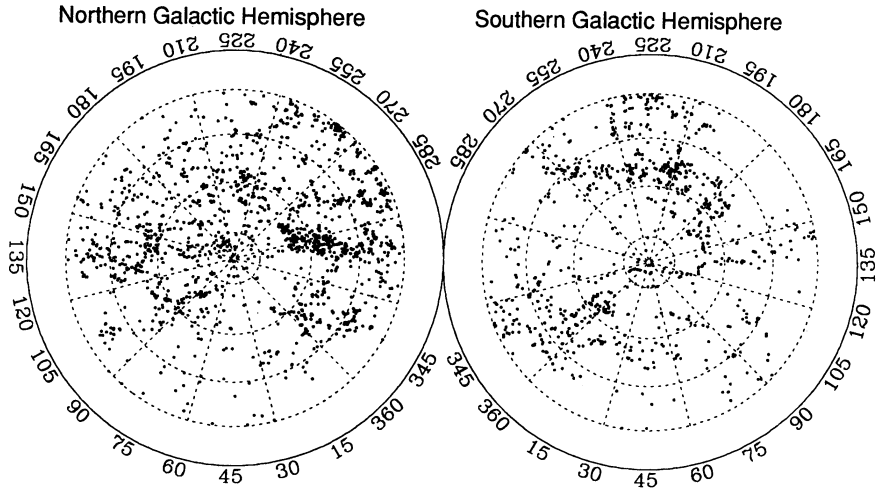

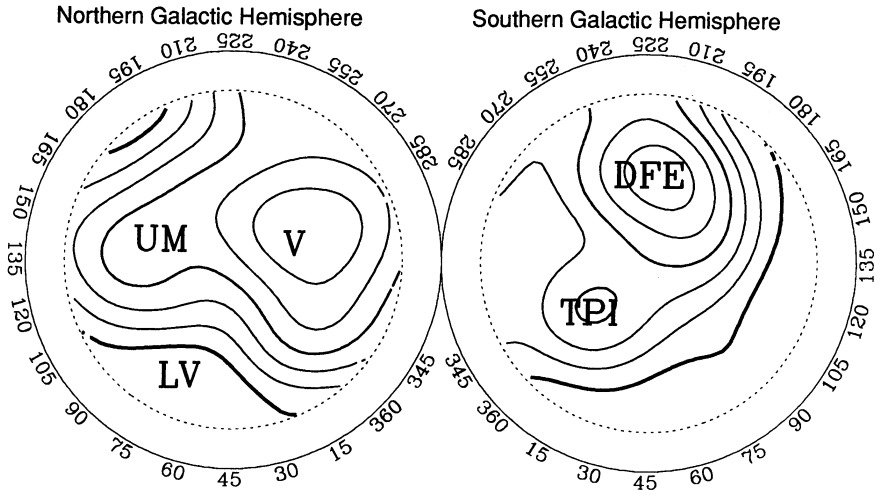

FIG. 7a

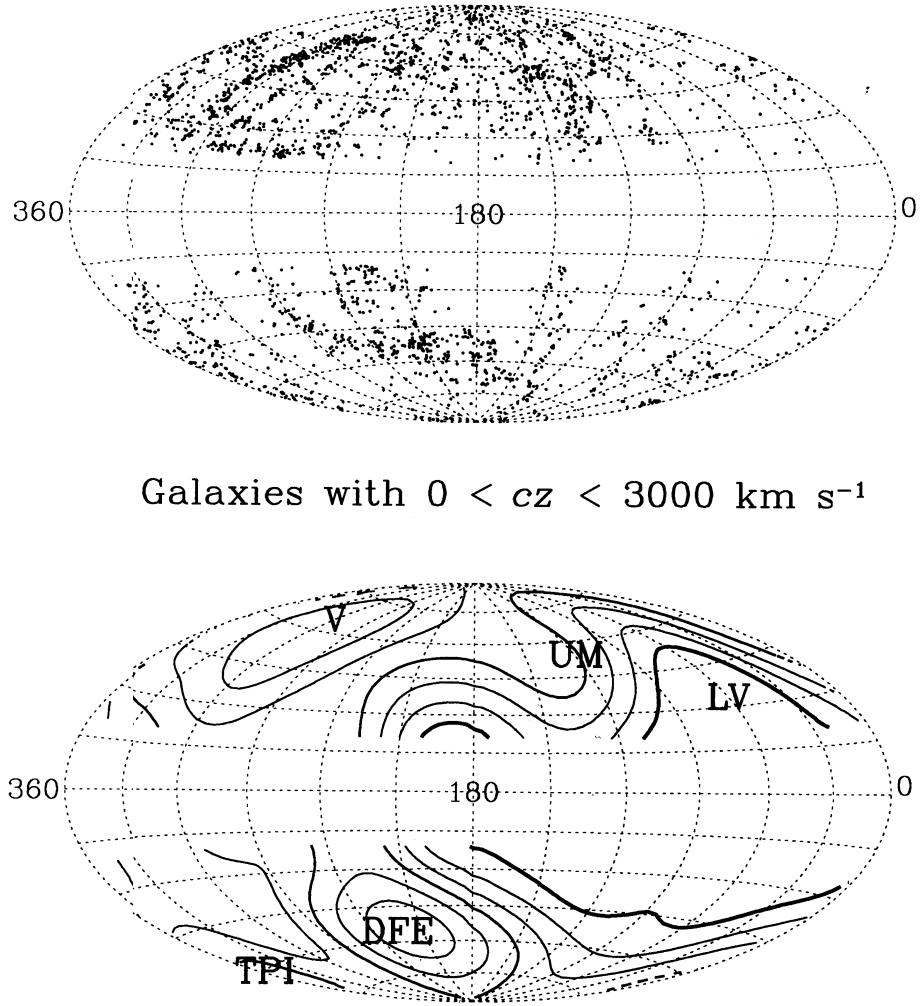

FIG. 7b

FIG. 7.—(*a*) The upper panel is as in Fig. 6*a*, but now showing only those galaxies with redshifts between 0 and 3000 m s^{-1}. The lower panel shows the galaxy density field in the redshift shell at 1500 km s^{-1}. The heavy solid contour is at mean density; the dashed contours are at $-\frac{1}{3}$ and $-\frac{2}{3}$ the mean density, and overdense regions are indicated by solid contours logarithmically spaced so that three contour levels represents an increase of a factor of 2. Several features of the density field are marked: V = Virgo Cluster, UM = Ursa Major cluster, DFE = Doradus-Fornax-Eridanus complex, TPI = Telescopium-Pavo-Indus supercluster foreground, and LV = Local void. (*b*) As in (*a*) with Aitoff projection.

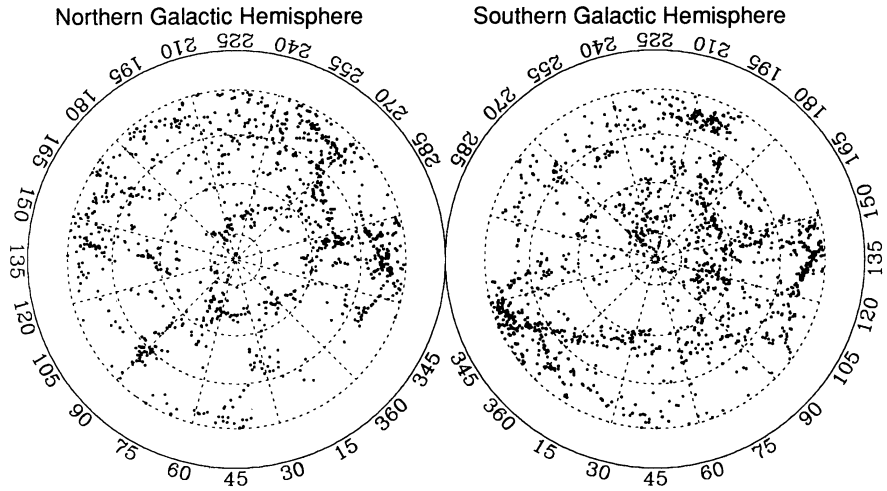

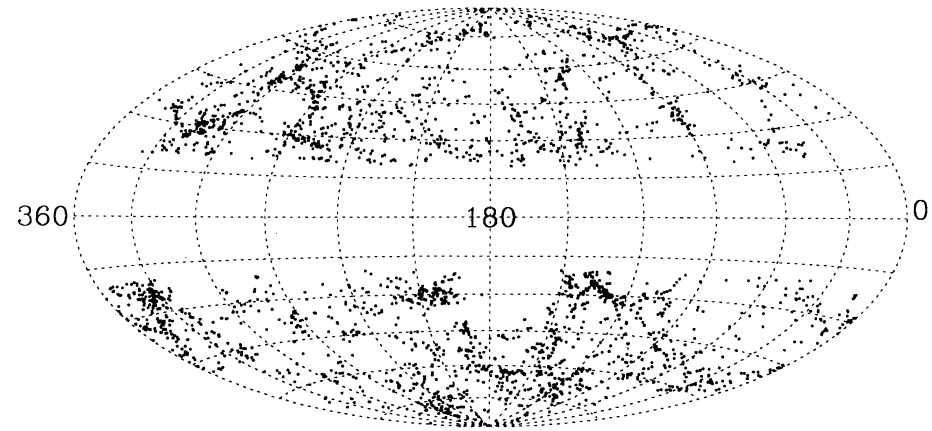

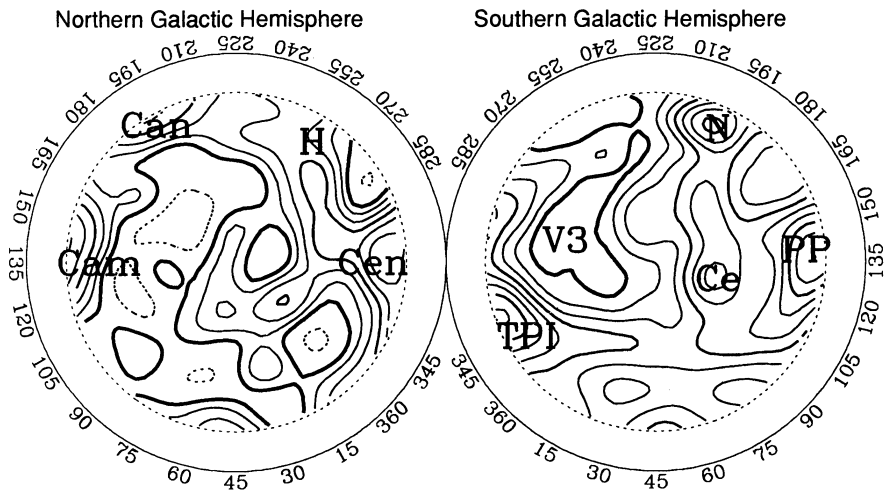

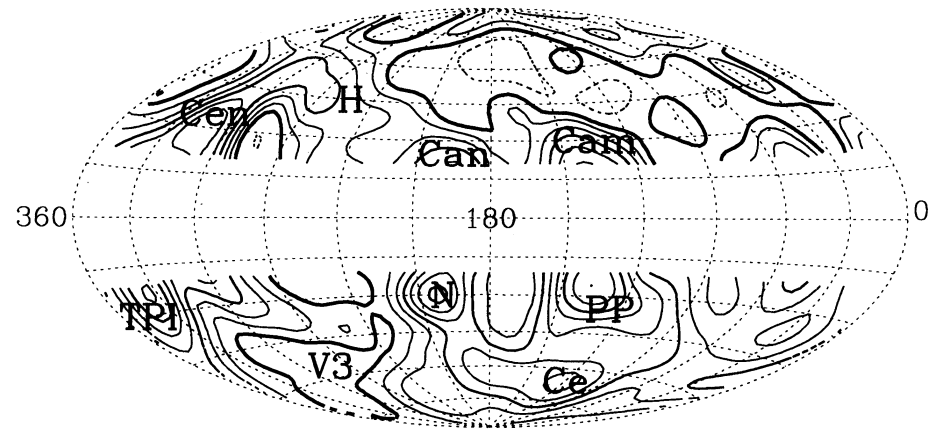

FIG. 8a

FIG. 8b

FIG. 8.—(*a*) As in Fig. 7*a*, now including galaxies between 3000 and 6000 km s^{-1} and showing the galaxy density field at 4500 km s^{-1}. The structures marked are the TPI supercluster; N = N1600; H = Hydra; Cen = Centaurus; Ce = Cetus; Cam = Camelopardalis; Can = Cancer; and V3 = Void 3 of da Costa et al. (1988). (*b*) As in (*a*) in Aitoff projection.

km s^{-1}. The lower panels show the smoothed galaxy density field on the spherical shell with radius 1500 km s^{-1}. The heavy contour is at the mean density, the dotted contours are at $\frac{1}{3}$ and $\frac{2}{3}$ the mean density, and the solid contours represent positive density contrasts with logarithmic spacing; three contours are a factor of 2 overdense. Note that the coordinate grid used in the upper panel of Figure 7*a* is not included in the lower panel, for clarity. The labels refer to various structures visible in these plots. The densest part of the Local Supercluster is the strong overdensity at $l = 300°$–$315°$, $b = 30°$–$70°$; the Virgo Cluster (V) is at its northern tip. The Ursa Major cluster ($l = 140°$, $b = 60°$, UM) is also visible, also in the supergalactic plane; indeed, galaxies are concentrated to the supergalactic plane all across the northern galactic hemisphere. Several other noticeable clumps belong to the Local Supercluster, among them the Leo ($l = 225°$, $b = 60°$), Virgo-Libra ($l = 345°$, $b = 35°$) and Canes Venatici-Camelopardalis ($l = 95°$, $50° < b < 70°$) clouds (see Tully & Fisher 1987). All these clouds are too small to appear in the contour plots at this smoothing. The Dorado-Fornax-Eridanus complex (DFE; the southern supercluster of Mitra 1989) ranges from $l = 190°$, $b = -60°$ to $l = 270°$, $b = -40°$, and the foreground of the TPI supercluster appears at $330° < l \leq 15°$, $-50° \leq b \leq -20°$. The Local void (LV) of Tully & Fisher (1987) is reflected in the paucity of galaxies at low Galactic longitudes. There is a void at $l = 285°$, $b = -60°$ named V1 by da Costa et al. (1988) visible in the galaxy distribution; its center is at 2500 km s^{-1}, and thus it is not apparent in the contour plots. Detailed maps of these foreground structures, in both hemispheres, can be found in Tully & Fisher (1987). See also Pellegrini et al. (1990) for a detailed discussion of the cosmography in the Southern Hemisphere.

Figures 8*a* and 8*b* show the galaxy distribution in the slice from 3000 to 6000 km s^{-1}, and the smoothed density field at 4500 km s^{-1}. This is the redshift interval which the ORS samples most completely (Fig. 4). In particular, this slice intersects the Great Attractor, which includes the TPI supercluster stretching from $l = 330°$, $b = -20°$ to $l = 30°$, $b = -60°$, and the Hydra-Centaurus supercluster [Hydra (H): $l = 255°$–$275°$, $b = 30°$; Centaurus (Cen): $l = 300°$–$320°$, $b = 25°$–$45°$]. The Pisces-Perseus supercluster (PP in the figure), studied in detail by Haynes & Giovanelli (1988), is on the opposite side of the sky at $l = 110°$–$150°$, $-35° \leq b \leq -20°$, and the N1600 group (represented by an N in the figures) at $l = 200°$, $b = -25°$. The latter is within the ESGC strip. There is some evidence for a connection between the Pisces-Perseus and TPI superclusters, especially visible in Figure 8*a*. The Cetus wall (Ce) stretches from $l = 120°$ through $l = 180°$, to the west of the southern Galactic pole. The void at $l = 300°$, $b = -45°$ was called V3 by da Costa et al. (1988). The northern sky is dominated by filamentary patterns and voids (Davis et al. 1982). The Camelopardalis-A569 ($l = 145°$, $b = 30°$; CAM) region is an overdensity which may be contiguous with the Pisces-Perseus supercluster (Hudson 1992), and the Cancer cluster ($l = 195°$, $b = 25°$; CAN) is at the edge of the zone of avoidance. The extensive void covering most of the northern Galactic hemisphere between $l = 45°$ and $l = 195°$ lies between the Virgo Cluster and the Great Wall (GW) and was apparent in the CfA survey of Davis et al. (1982).

Figures 9*a* and 9*b* show the galaxy distribution from 6000 to 9000 km s^{-1}and the density field at 7500 km s^{-1}. The ORS is fast becoming sparse at these redshifts, and individual structures are difficult to discern. However, the Coma cluster and Abell 1367 (labeled Co) make up the overdensity centered on the north Galactic pole, and the structure of which this is a part, extending to $l = 245°$, $b = 55°$, and $l = 355°$, $b = 65°$, is the southern extension of the GW of de Lapparent, Geller, & Huchra (1986; 1988) and Geller & Huchra (1989), where it dips down to low redshifts. Saunders et al. (1991) defined the supercluster S5 at $l = 95°$, $b = -30°$.

3.2. *Distribution in Radius*

As mentioned above, most of the new redshifts for this project were measured in regions of the sky not previously surveyed: the ESGC strip and the two strips defined by $20° < |b| < 30°$. Thus, we discuss the galaxy distribution in these three regions in some detail.

Figures 10 and 11 show the strips with $-30° \leq b \leq -20°$ and $20° \leq b \leq 30°$, respectively. These strips are parallel to the zone of avoidance and so span 360° in the sky. Galactic longitude is the angular coordinate in these plots; Galactic latitude has been suppressed. Our Local Group is in the center of each plot, and redshift distance runs radially towards the edge. The velocities are again in the Local Group frame; no further corrections for peculiar velocities were applied. The dashed circles have radii of 2000, 4000, and 6000 km s^{-1}; the outer circle has a radius of 8000 km s^{-1}. Regions heavily affected by Galactic extinction are indicated by the pie-shaped wedges (compare with Fig. 5*a*).

Figure 10 is dominated by two superclusters: the Pisces-Perseus supercluster spanning the range $125° \leq l \leq 155°$ and with redshifts ranging from 4000 to 6000 km s^{-1}, and the TPI supercluster, concentrated at $l = 330°$ and 4000 km s^{-1}, and with an extension between 4000 and 6000 km s^{-1} to $l = 0°$. The galaxy concentration at $l = 200°$, $v = 4500$ km s^{-1} is the N1600 region (Saunders et al. 1991), while the extended structure at $l = 225°$, $v = 3500$ km s^{-1} is a supercluster named S1 by Saunders et al. (1991). Another of these superclusters, named S5, is seen at $l = 95°$, $v = 7000$ km s^{-1} and seems to be connected to the Pisces-Perseus supercluster.

The galaxy distribution in Figure 11 is also quite nonuniform, with galaxies concentrated in large lumps surrounded by voids. The figure is dominated by the Virgo-Hydra-Centaurus region, which occupies the interval $260° \leq l \leq 310°$ and 2000 km s^{-1} $\leq v \leq$ 4500 km s^{-1}. The clump at $l = 260°$, 3000 km s^{-1} is Abell 1060, and that at $l = 315°$, 4000 km s^{-1} consists of Abell 3526, 3560, and 3565 in the Hydra-Centaurus region. Also visible are the Abell 569 supercluster ($l = 170°$, $v = 6000$ km s^{-1}), the Camelopardalis supercluster ($l = 135°$, $v = 4500$ km s^{-1}) and the Cancer cluster ($l = 195°$, $v = 4500$ km s^{-1}) (see also Hudson 1992). The concentration of galaxies to the supergalactic plane (crossing the panel from $l = 135°$ to $l = 315°$) is quite dramatic: notice the large void at $l = 260°$–$300°$ and redshifts beyond 4000 km s^{-1}, as well as the paucity of galaxies at $l = 70°$–$120°$ at all redshifts in this slice.

In Figure 12 we show the ESGC strip. The two nearly opposite regions completely devoid of galaxies are the intercepts with the plane of the Galaxy. As we saw in Figure 4, the ESGC strip is more densely sampled than is the rest of the sky, making dense regions stand out more clearly than in Figures 10 and 11. The radially extended feature at $\alpha = 13^h$ is a piece of the Virgo-Hydra-Centaurus complex, particularly by the Centaurus group ($v = 2500$ km s^{-1}) and the Virgo southern extension ($v = 1000$ km s^{-1}). Opposite to it ($2^h \leq \alpha \leq 3^h$, $v = 2000$ km s^{-1}) is the continuation of the Fornax-Eridanus complex toward the equator. Nearly in the same direction but in the

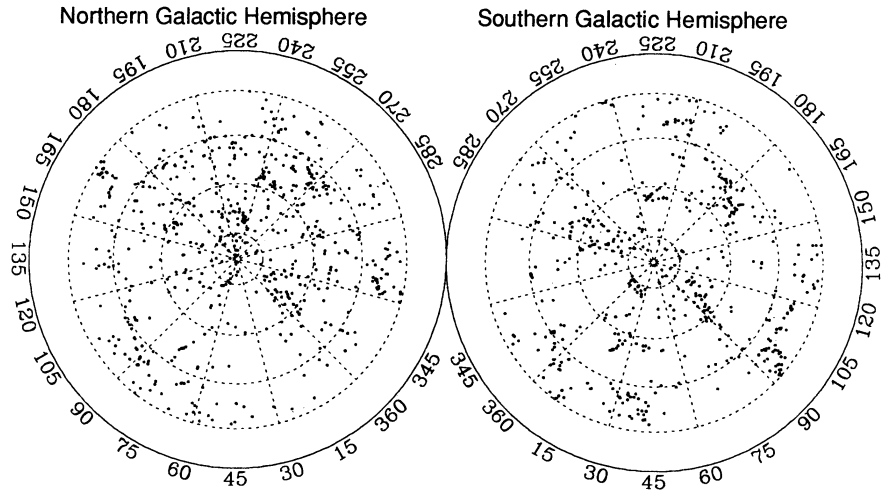

Galaxies with $6000 < cz < 9000$ km s^{-1}

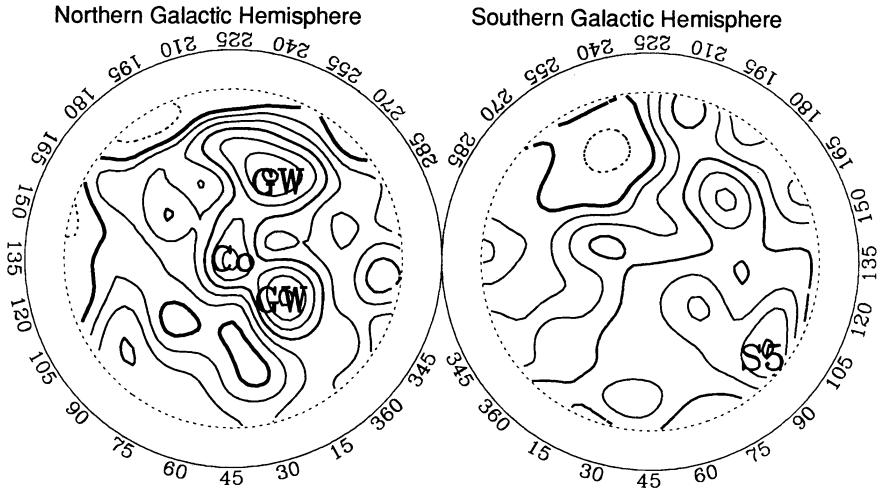

Redshift Shell at 7500 km s^{-1}

FIG. 9a

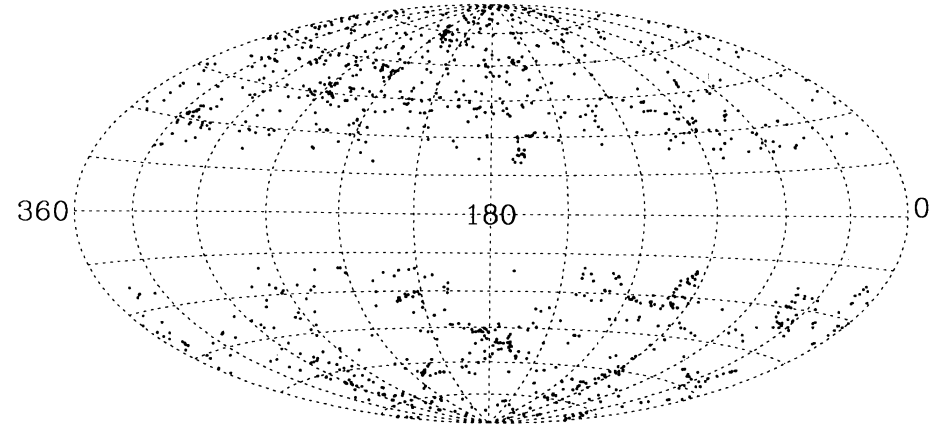

Galaxies with $6000 < cz < 9000$ km s^{-1}

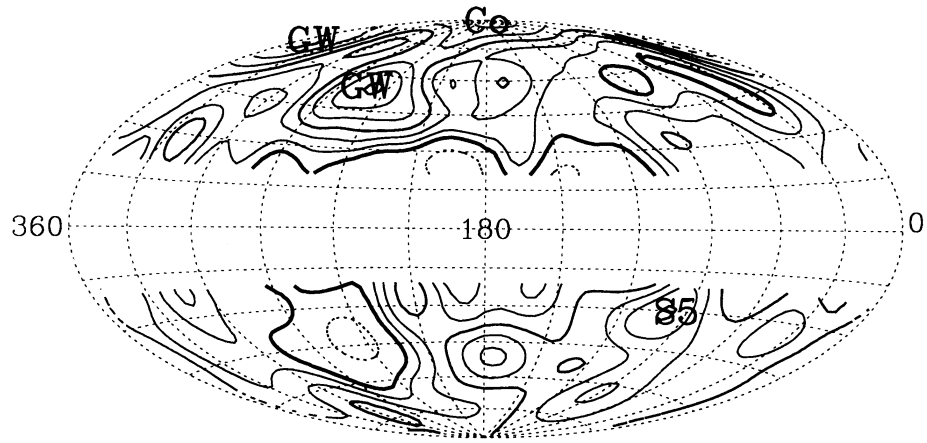

Redshift Shell at 7500 km s^{-1}

FIG. 9b

FIG. 9.— As in Fig. 8*a*, now including galaxies between 6000 and 9000 km s^{-1} and showing the galaxy density field at 7500 km s^{-1}. The structures marked are: Co = Coma-A1367; GW = southern extension of the Great Wall, S5 = supercluster 5 of Saunders et al. (1991). (*b*) As in (*a*) in Aitoff projection.

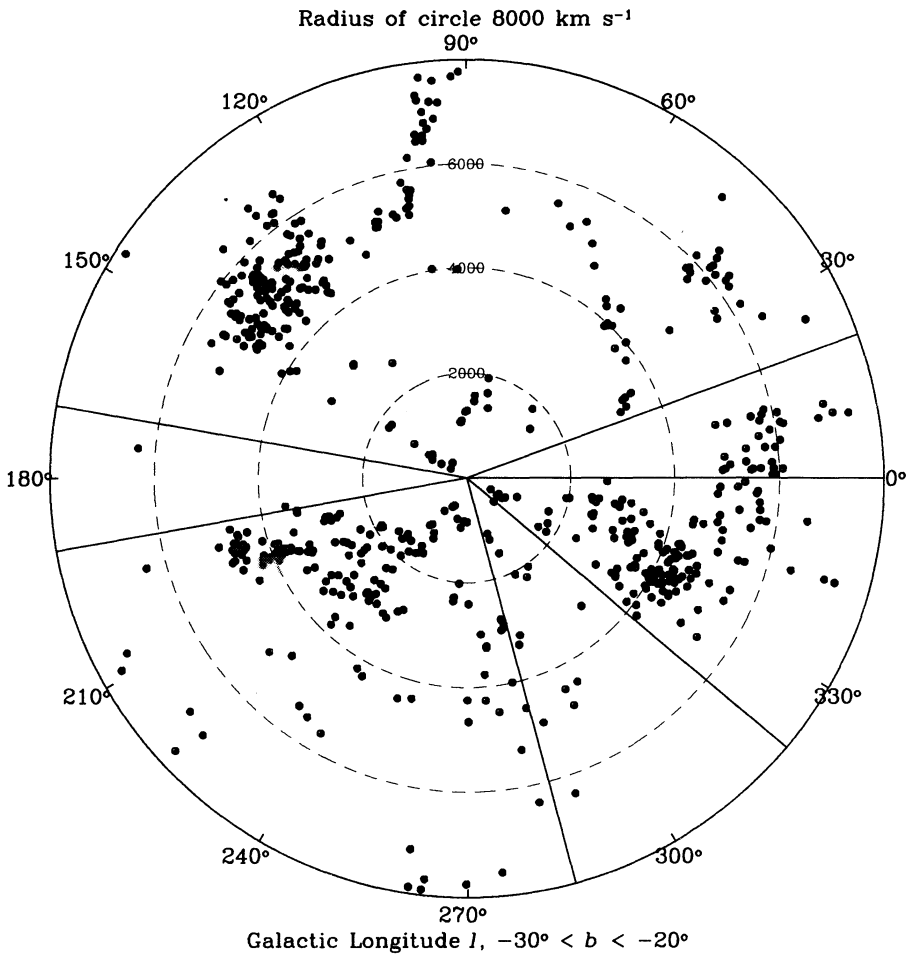

FIG. 10.—The slice corresponding to $-30° \leq b \leq -20°$ out to 8000 km s^{-1}. Galactic longitude runs azimuthally in the counterclockwise direction. The Local Group lies in the center of the plot. Redshift distances, corrected for our motion relative to the Local Group, increase radially outward. The dashed circles are drawn at 2000, 4000, and 6000 km s^{-1}. The pie-shaped wedges correspond approximately to regions of high Galactic extinction (compare Fig. 5*a*).

background, there is a very extended linear feature ranging from $\alpha = 0^h$ to $\alpha = 4^h$. This is the northern extension of the Cetus Wall, as mapped by the SSRS (da Costa et al. 1988) and the MCG Equatorial Survey (Huchra et al. 1993); see da Costa et al. (1994). The latter authors hpothesize that this structure is contiguous with the Pisces-Perseus supercluster. In fact, this connection can also be seen in Figure 8. To the east, there is a prominent structure at $\alpha = 5^h$, but in fact this is not to be identified with any single cluster; although it is close to N1600, it is spread out over some 100 square degrees.

4. DISCUSSION

In this paper we have presented a sample of optical galaxies covering most of the celestial sphere and with almost complete redshift information. The ORS provides a dense sampling of the structures that dominate the density field in the Local universe out to 8000 km s^{-1}. Among the new areas surveyed by ORS are the regions close to the plane of the Galaxy and the ESGC strip. The galaxy distribution in these regions is shown in greater detail and completeness than in earlier surveys. In particular, the Virgo supercluster, the Doradus-Fornax-Eridanus complex, Hydra-Centaurus supercluster, the TPI supercluster, and the low-redshift component of the GW are all apparent in the data.

Given its high density sampling and large sky coverage, the ORS is well suited for a quantiative analysis of the density field as traced by bright optical galaxies and of its dependence on various parameters. Particularly important will be the comparison of the ORS density field with that described by *IRAS* galaxies, to address the question of whether determinations of the cosmological density parameter from these samples are consistent. Utilization of a composite *IRAS*-optical sample may be useful for deriving the peculiar velocity field and constraining the bias and density parameters.

A density field analysis of optical galaxies has recently been carried out by Hudson (1993a), who used the entire ESO and UGC catalogs, but with incomplete redshift information. In addition, unlike the present sample, Hudson had no information about the galaxy distribution in the ESGC strip. The density field described here is qualitatively similar to that presented by Hudson. He finds that optically selected galaxies show stronger clustering than do *IRAS* galaxies by a factor of ~ 1.5 on 800 km s^{-1} scales; some indication for morphological segregation is also observed.

Another optically selected redshift survey has been carried out by Freudling & da Costa (1994). This sample contains about 5800 objects limited to $m_B \leq 14.5$ in the regions $b \geq 40°$ and $b \leq -30°$. They are making models for the peculiar velocity

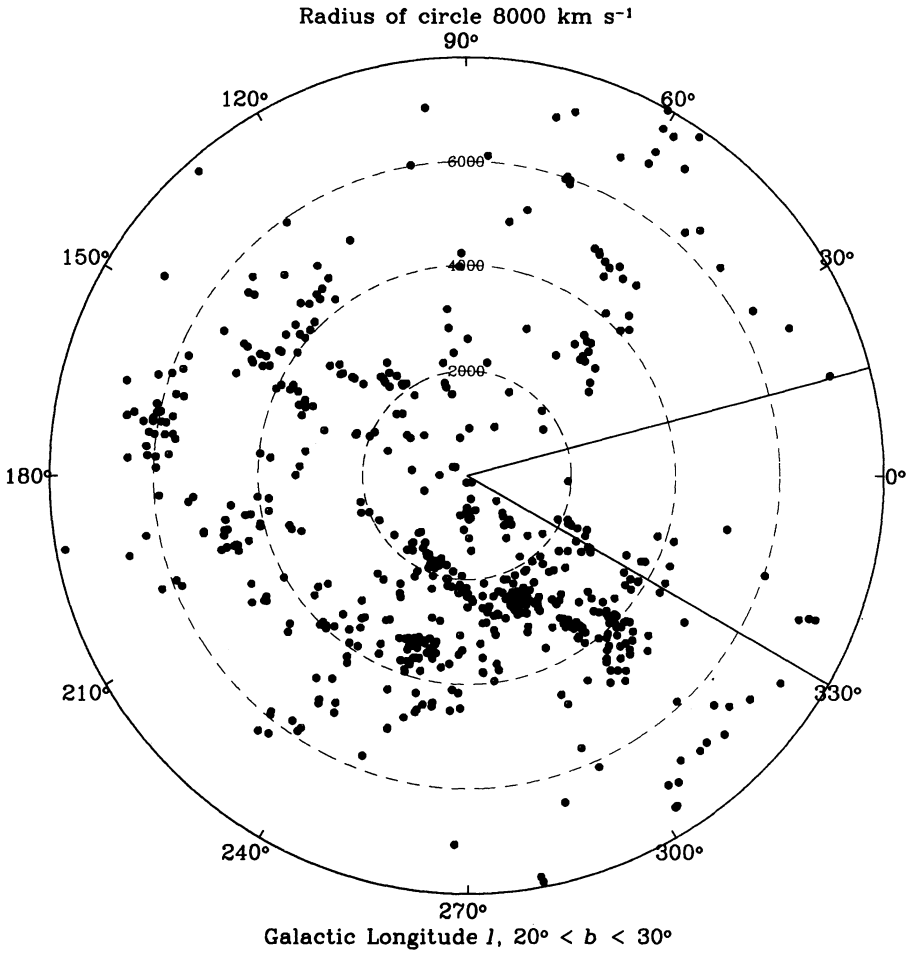

FIG. 11.—As in Fig. 10, for the slice $20° \leq b \leq 30°$

field as inferred from this optical sample in combination with *IRAS* (see Freudling, da Costa, & Pellegrini 1994).

There are two developments on the horizon that should allow the selection criteria of the present sample to be tightened considerably. B. Madore and G. Helou are carrying out a photometric CCD survey in the *R* band of 10,000 galaxies based on the sample selection criteria here. These data will give accurate diameters and magnitudes for all galaxies in the present survey, allowing a much tighter selection. In addition, D. Lynden-Bell and collaborators have carried out an Automatic Plate Measuring Facility (APM) galaxy survey in the ESGC strip that will be complete to $\theta_B \geq 0.4$ or $m_B \leq 17$; all galaxies have been scanned from the APM plates, yielding a database as rich as that of ESO-LV, but extending substantially deeper.

ORS is affected by variable amounts of Galactic absorption across the sky. Systematic selection effects as a function of direction in the sky may also arise due to inconsistencies among the different magnitude and diameter systems used in defining the sample (see Fig. 2). We present methods for correcting for these effects, and creating a well-defined density field, in Paper II of this series. Once this is done, the scientific questions which we hope to address with the present sample include:

1. Are there significant variations in the large-scale galaxy distribution as a function of morphology, spectral properties, or surface brightness? In particular, are there significant differences in the density fields of *IRAS* and optical galaxies?

2. What is the amount of relative biasing in the galaxy distribution, and how does it depend on scale? Is relative biasing nonlinear?

3. What are the high-order clustering properties of the galaxy distribution? More specifically, do they confirm the scale-invariant hypothesis and, if so, on what scales?

4. What is the dimensionality, density contrast, and extent of the Local Supercluster?

We intend to tackle all the above questions in upcoming papers.

Harold Corwin deserves special thanks for his enormous efforts in producing the ESGC, making it available to us well in advance of publication, and for much help and useful advice throughout this project. We would also like to thank Barry Madore, Donald Lynden-Bell, Dave Burstein, and Will Saunders for their advice in many aspects of this project and useful discussions. Nicolaci da Costa was particularly generous with redshifts in advance of publication. Amber Miller assisted with the data reduction. Robert Lupton wrote the software package used to generate the figures and cheerfully made improvements in the code when we requested them. The telescope operators of Lick, Mount Hopkins, Las Campanas, Palomar, and Cerro Tololo Observatories all did their usual superb jobs. M. A. S. is

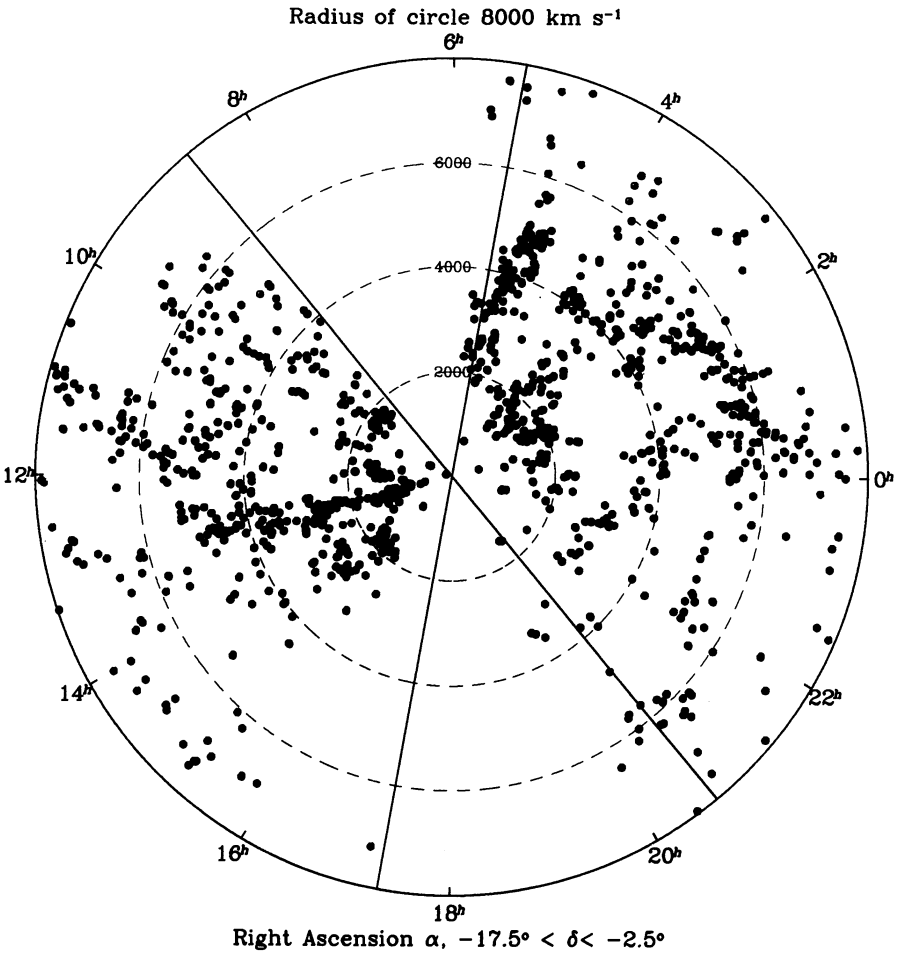

FIG. 12.—As in Fig. 10, for the ESGC strip $-17°.5 \leq \delta \leq -2°.5$

supported at the IAS under NSF grant PHY 92-45317 and grants from the W. M. Keck Foundation and the Ambrose Monell Foundation. M. D. acknowledges the support of NSF grant AST 92-21540. This research has made use of the NASA/IPAC Extragalactic Database (NED) which is operated by the Jet Propulsion Laboratory, Caltech, under contract with the National Aeronautics and Space Administration. B. X. S. acknowledges a doctoral fellowship from the Conselho Nacional de Desenvolvimento Científico e Tecnológico (CNPq) and the generous hospitality of the Caltech Astronomy department. B. X. S. and O. L. thank the Institute for Advanced Study for its invitations to visit.

REFERENCES

Bouchet, F. R., Davis, M., Strauss, M. A., Fisher, K. B., Yahil, A., & Huchra, J. P. 1993, ApJ, 417, 36
Burstein, D., & Heiles, C. 1982, AJ, 87, 1165
Corwin, H. G., & Skiff, B. A. 1994, in preparation (ESGC)
da Costa, L. N., Pellegrini, P., Davis, M., Meiksin, A., Sargent, W., & Tonry, J. 1991, ApJS, 75, 935
da Costa, L. N., et al. 1988, ApJ, 327, 544
———. 1994, ApJ, 424, L1
Davis, M., Huchra, J., Latham, D. W., & Tonry, J. 1982, ApJ, 253, 423
Dekel, A. 1994, ARA&A, 32, 371
Dekel, A., Bertschinger, E., Yahil, A., Strauss, M. A., Davis, M., & Huchra, J. P. 1993, ApJ, 412, 1
de Lapparent, V., Geller, M. J., & Huchra, J. P. 1986, ApJ, 302, L1
———. 1988, ApJ, 332, 44
de Vaucouleurs, G., de Vaucouleurs, A., Corwin, H., Buta, R., Paturel, G., & Fouqué, P. 1991, Third Reference Catalogue of Bright Galaxies (New York: Springer)
Dressler, A. 1991, ApJS, 75, 241
Fasano, G. 1985, A&AS, 60, 285
Fisher, K. B., Huchra, J. P., Strauss, M. A., Davis, M., Yahil, Y., & Schlegel, D. 1995, ApJS, in press
Fisher, K. B., Davis, M., Strauss, M. A., Yahil, A., & Huchra, J. P. 1994a, MNRAS, 266, 50
———. 1994b, MNRAS, 267, 927
Fouqué, P., & Paturel, G. 1985, A&A, 150, 192
Freudling, W., & da Costa, L. N. 1994, in Cosmic Velocity Fields, ed. F. R. Bouchet & M. Lachièze-Rey (Gif sur Yvette: Editions Frontières), 187
Freudling, W., da Costa, L. N., & Pellegrini, P. S. 1994, MNRAS, 268, 943
Geller, M. J., & Huchra, J. P. 1989, Science, 246, 897
Haynes, M. P., & Giovanelli, R. 1988, in Large-Scale Motions in the Univese: A Vatican Study Week, ed. V. C. Rubin & G. V. Coyne (Princeton: Princeton University Press), 31
Huchra, J., Davis, M., Latham, D., & Tonry, J. 1983, ApJS, 52, 89
Huchra, J., Geller, M. J., de Lapparent, V., & Corwin, H. 1990, ApJS, 72, 433
Huchra, J., Latham, D. W., da Costa, L. N., Pellegrini, P. S., & Willmer, C. N. A. 1993, AJ, 105, 1637
Hudson, M. J. 1992, Ph.D. thesis, Univ. Cambridge
———. 1993a, MNRAS, 265, 43
———. 1993b, MNRAS, 266, 475
Hudson, M., Dekel, A., Courteau, S., Faber, S. M., & Willick, J. A. 1995, MNRAS, in press
Hudson, M. J., & Lynden-Bell, D. 1991, MNRAS, 252, 219 (HLB)
IRAS Catalogs & Atlases, Explanatory Supplement. 1988, ed. C. A. Beichman et al. (Washington: U.S. Govt. Printing Office)
Kaiser, N., Efstathiou, G., Ellis, R., Frenk, C., Lawrence, A., Rowan-Robinson, M., & Saunders, W. 1991, MNRAS, 252, 1
Kron, G. E., & Shane, C. D. 1976, A&SS, 39, 401
Lahav, O. 1987, MNRAS, 225, 213

Lahav, O., Nemiroff, R. J., & Piran, T. 1990, ApJ, 350, 119
Lahav, O., Rowan-Robinson, M., & Lynden-Bell, D. 1988, MNRAS, 234, 677
Lahav, O., & Saslaw, W.1992, ApJ, 396, 430
Lauberts, A. 1982, The ESO-Uppsala Survey of the ESO(B) Atlas (München: European Southern Obs.)
Lauberts, A., & Valentijn, E. 1989, The Surface Photometry Catalogue of the ESO-Uppsala Galaxies (München: European Southern Obs.) (ESO-LV)
Lawrence, A., et al. 1994, MNRAS, in preparation
Loveday, J., Peterson, B. A., Efstathiou, G., & Maddox, S. J. 1992, ApJ, 390, 338
Lynden-Bell, D., Lahav, O., & Burstein, D. 1989, MNRAS, 241, 325 (LLB)
Mitra, S. 1989, AJ, 98, 1175
Nilson, P. 1973, Uppsala General Catalogue of Galaxies, Uppsala Astron. Obs. Ann., 6 (UGC)
Paturel, G. 1977, A&A, 56, 259
Paturel, G., Fouqué, P., Lauberts, A., Valentijn, E. A., Corwin, H. G., & de Vaucouleurs, G. 1987, A&A, 184, 86
Paturel, G., Petit, C., Kogoshvili, N., Dubois, P., Bottinelli, L., Fouqué, P., Garnier, R., & Gouguenheim, L. 1991, A&AS, 91, 371
Pellegrini, P. S., da Costa, L. N., Huchra, J. P., Latham, D. W., & Willmer, C. 1990, AJ, 99, 751
Rowan-Robinson, M., et al. 1990, MNRAS, 247, 1
Sandage, A., & Tammann, G. A. 1981, Revised Shapley-Ames Catalog (Washington: Carnegie Inst. of Washington) (RSA)
Santiago, B. X., & Strauss, M. A. 1992, ApJ, 387, 9
Santiago, B. X., Strauss, M. A., Lahav, D., Davis, M., Dressler, A., & Huchra, J. P. 1995, ApJ, submitted (Paper II)
Saunders, W., et al. 1991, Nature, 349, 32
Saunders, W., Rowan-Robinson, M., & Lawrence, A. 1992, MNRAS, 258, 134
Saunders, W., et al. 1995a, in preparation
———. 1995b, in 35th Herstmonceux Conference on Wide Field Spectroscopy, ed. S. J. Maddox & A. Aragón-Salamanca (Cambridge: Cambridge Univ. Press), in press
Scharf, C., Hoffman, Y., Lahav, O., & Lynden-Bell, D. 1992, MNRAS, 256, 229
Scharf, C., & Lahav, O. 1993, MNRAS, 264, 439
Schechter, P. L. 1976, ApJ, 203, 297
Strauss, M. A. 1993, in Sky Surveys: Protostars to Protogalaxies, ed. B. T. Soifer (ASP Conf. Ser., 43), 153
Strauss, M. A., Davis, M., Yahil, A., & Huchra, J. P. 1990, ApJ, 361, 49
———. 1992a, ApJ, 385, 421
Strauss, M. A., Huchra, J. P., Davis, M., Yahil, A., Fisher, K. B., & Tonry, J. P. 1992b, ApJS, 83, 29
Strauss, M. A., & Willick, J. 1995, Phys. Rep., in press
Strauss, M. A., Yahil, A., Davis, M., Huchra, J. P., & Fisher, K. B. 1992c, ApJ, 397, 395
Tully, R. B., & Fisher, J. R. 1987, Nearby Galaxies Atlas (Cambridge: Cambridge Univ. Press)
Vorontsov-Velyaminov, B. A., Archipova, V. P., & Krasnogorskaja, A. A. 1962–1974, Morphological Catalogue of Galaxies Vols. 1–5 (Moscow: Moscow State Univ.) (MCG)
Yahil, A., Tammann, G. A., & Sandage, A. 1977, ApJ, 217, 903
Yahil, A., Sandage, A., & Tammann, G. A. 1980, ApJ, 242, 448
Yahil, A., Strauss, M. A., Davis, M., & Huchra, J. P. 1991, ApJ, 372, 380
Zwicky, F., et al. 1961–1968, Catalog of Galaxies and Clusters of Galaxies, Vols. 1–6 (Pasadena: California Inst. of Technology) (CGCG)